INVESTIGATION OF SUPERSONIC AIR PLASMA JET PRODUCED IN THE VKI PLASMATRON FACILITY

Damien Lequang, Yacine Babou, Olivier Chazot, Pascal André

INVESTIGATION OF SUPERSONIC AIR PLASMA JET PRODUCED IN THE VKI PLASMATRON FACILITY

D. Le Quang[1], Y. Babou[1], O. Chazot[1], and P. André[2]

[1]*Aeronautics and Aerospace Department, von Karman Institute for Fluid Dynamics, Chaussée de Waterloo 72, 1640 Rhode-Saint-Genèse, Belgium.*
[2]*Electric arc and thermal plasmas, LAEPT, 24 avenue des Landais Aubière - France.*

ABSTRACT

Thermodynamic characterization of a supersonic air plasma jet produced in the VKI Plasmatron facility is presented. Plasma flow regimes corresponding to underexpanded and highly underexpanded situations are investigated by means of Optical Emission Spectroscopy (OES) technique. Several diagnostics are presented using both molecular and atomic radiative contributions. Electron density, excitational energy distribution and molecular spectra fitting are presented.

Key words: Emission spectroscopy; Supersonic air plasma.

1. INTRODUCTION

During hypersonic atmospheric entries, the radiative heating experienced by a vehicle is a major issue for accurate prediction of thermal heat flux. Comparison of predictive computations with detailed description of kinetic processes experimentally investigated are mandatory to assess the reliability of nonequilibrium kinetic models. Due to the relatively large cost of missions and the difficulty of performing accurate measurements in flight, plasma source ground test facilities have been developed. The use of supersonic plasma jets to investigate non equilibrium processes is widely reported but most investigations deal with mono-atomic gases (Sember & al.[V.S02], Selezneva & al.[S.E01], Sanden & al. [M.C93], Drake & al. [D. 08] [D. 09] and Robin & al. [L.R94]). Supersonic plasma expansion are characterized by a rapid cooling and recombination which result in kinetic non equilibrium. Although Optical Emission Spectroscopy (OES) technique is convenient to investigate nonequilibrium plasma flows, characterization have to be carried out using cautious assumptions. Indeed, Sember & al. [V.S02] outlined that spectroscopic analysis might give questionable results due to non Boltzmann excited states distribution. Present investigation is carried out using the Inductively Coupled Plasma (ICP) Plasmatron facility operating with air mixture. The discussion is focused on the interpretation of spectroscopic measurements performed in the first expansion-compression structure of supersonic underexpanded plasma jets. Preliminary investigation of the plasma source performance was executed to insure high quality measurements. Comprehensive characterization of the flow by means of high speed imaging has been executed to identify suitable operating conditions in order to perform (OES). Operating the Plasmatron at constant power of 490 kW and 4.5 g/s mass flow rate, the pressure in the ignition region is maintained at 120 mbar. Expansion is performed through a sonic throat into a low pressure chamber. Two back pressure conditions ensuring low influence of power feeding oscillation on plasma emission, good signal to noise ratio and strong hydrodynamic gradients have been selected and correspond to 12 and 6 mbar chamber pressure. In section 2, experimental arrangement and spectra processing are presented. In section 3, spectroscopic diagnostics based on atomic and molecular contributions are detailed. Electron density, rotational temperature and excitational energy distribution are presented in section 4. Preliminary discussion are developed in 5.

2. EXPERIMENTAL ARRANGEMENT AND SPECTRA PROCESSING

2.1. Plasmatron facility and supersonic plasma jet generation

The VKI Plasmatron Inductively Coupled Plasma (ICP) source uses a high frequency, high power and high voltage generator (400 kHz, 1.2 MW, 11 kV), feeding a single-turn inductor [B. 97], [B. 00]. For the present experiments, the Plasmatron is operating at 490 kW power and 4.5 g/s mass flow rate. Supersonic plasma jet are obtained by expanding the plasma through a convergent nozzle (35 mm throat diameter) into a chamber maintained at low pressure. In the present study, the pressure in the chamber is maintained at 6 or 12 mbar corresponding respectively to a highly underexpanded (figure 1) and underexpanded figure (2) situation while the pressure in the reservoir is maintained at 120 mbar. A basic analysis of emission oscillation shows that typical fluctuations

(induced by three phase rectifier at 600 and 1200 Hz) usually observed in subsonic regime are damped and lower frequency peaks rise at 200 and 166 Hz. The super-
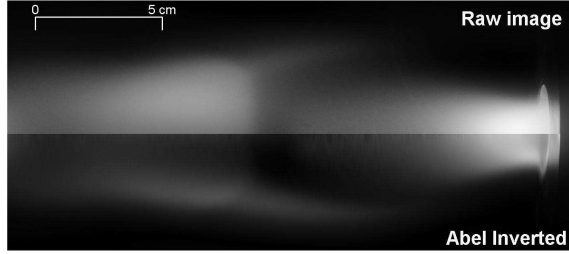

Figure 1. Supersonic air plasma jets - back pressure: 6 mbar.
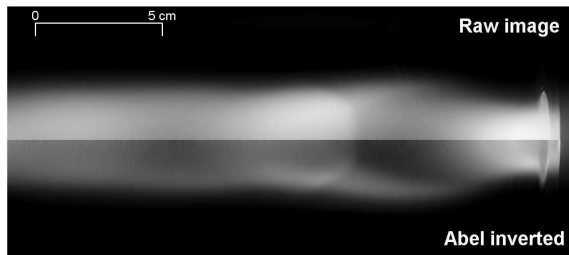

Figure 2. Supersonic air plasma jets - back pressure: 12 mbar.

sonic plasma flows encountered in this study evidence a pressure at the exit of the convergent being higher than in the chamber. In order to equilibrate the pressure difference at the exit of the convergent, expansion waves are created and directed towards the jet axis which are then reflected in the direction of the plasma jet boundaries. These expansion waves direct the flow towards the edge of the plasma jet, creating a radial expansion in addition to the axial expansion. The edges of the expansion zone are bright because of the reflection of the expanding flow by the cold dense surrounding gas, which gives rise to the so called barrel shocks. Reducing the chamber pressure, leads to the creation of a Mach disk downstream of the first expansion cell, leading to subsonic velocities downstream of this region with an increase of the local temperature and pressure. Abel inversion (figures 1 and 2) performed on raw images illustrates complex structures of compression and expansion zones in the jet caused by multiple reflections of expansion and shock waves. In particular, it evidences bright zones in the compression region mainly located on the edges. Through isentropic expansion calculations, we evaluate the Mach number in the expansion region before the shock using the expansion angle and assuming ideal air. The results are displayed figure 3.
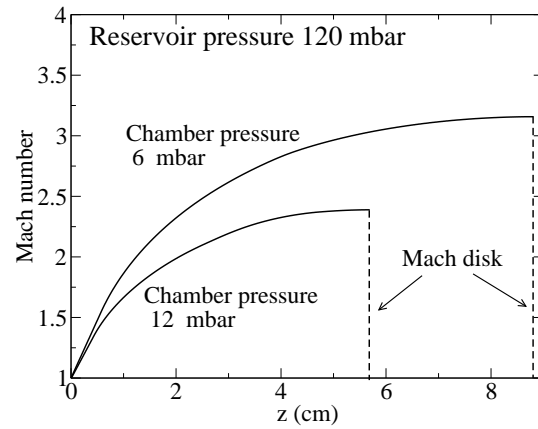

Figure 3. Mach number estimation in the expansion region before the shock.

2.2. Optical emission spectroscopy measurement

Optical Emission Spectroscopy (OES) allows to obtain information on excited states densities without disturbing the flow. Accurate measurements rely on stationary flow emission and low contamination of the jet. A conventional OES technique was set up and applied in a large spectral range on supersonic underexpanded air plasma jets in the first expansion zone (starting at 2.5 cm from the throat) and in the compression region. For clarity, figure 4 illustrates the location of axial measurements. Dashed lines correspond to 2.5, 3.5, 4.5, 8.5, 10.5, 11.5, 12.5, 13.5, 15.5, 17.5 cm (resp.2.5, 3.5, 4.5, 6.5, 7.5, 8.5, 9.5, 10.5, 11.5, 12.5 cm) axial locations for 6 mbar (resp. 12 mbar) back pressure case. At each axial location, the
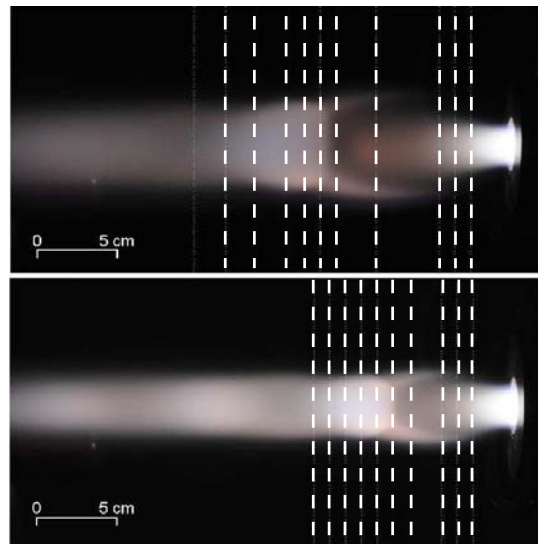

Figure 4. Axial location of spectroscopic measurements. 6 mbar (top), 12 mbar (bottom) back pressure.

line of sight plasma jet emission is collected through an

aperture and then focused with a fused silica lens onto the entry of a Acton Series monochromator of 75 cm focal lengths. The spectrometer is combined with a ICCD PI-MAX camera with a frame of 1024 × 1024 pixels of 12.8 μm side. Emission issued from the jet is spatially resolved in the radial direction. A radial slice of about 19 cm height was optically conjugated using a 100 mm focal lens onto an image with a magnification factor of 0.07. It allows to capture the whole radial profile of the jet onto the CCD screen of the camera with a spatial resolution of about 180 microns. We focus our study on the
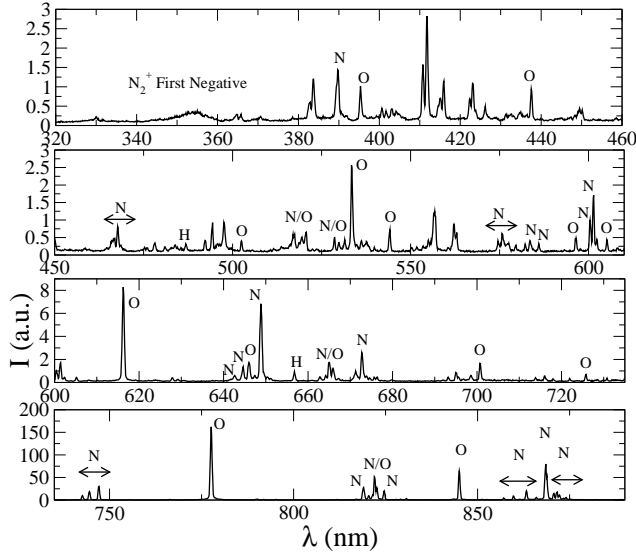
Figure 5. *Typical radiative signature of supersonic air plasma jet in the first expansion zone (r = 0 cm, z = 2.5 cm).*

visible spectral domain that includes mainly atomic contribution of oxygen and nitrogen atomic lines. The small contribution of N_2^+ First negative system, H_α and H_β hydrogen lines have also been investigated. The radiation from oxygen and nitrogen atomic lines and the N_2^+ First negative system were recorded using a 150 groves/mm grating as the hydrogen lines spectral resolution was improved by using a 1200 groves/mm grating in order to resolve the Stark broadening. The corresponding spectral resolutions were measured to be respectively 0.5 nm and 0.06 nm, setting the entrance slit of the monochromator to 3 microns. The recorded spectra were calibrated in absolute intensity combining a ribbon tungsten lamp and its documented absolute radiance and a deuterium source. Calibrated spectra at the plasma jet center line are shown in figure 5. At the conditions reported here, the air mixture is assumed to be optically thin and proper Abel inversion was applied on measured spectra allowing to rebuild the local spectral emission ($W.m^{-3}.sr^{-1}.\lambda^{-1}$).

On figures 6 and 7, mapping of the local emission integrated within [400-900] nm spectral range is displayed and show good agreement with pictures on figures 1 and 2.
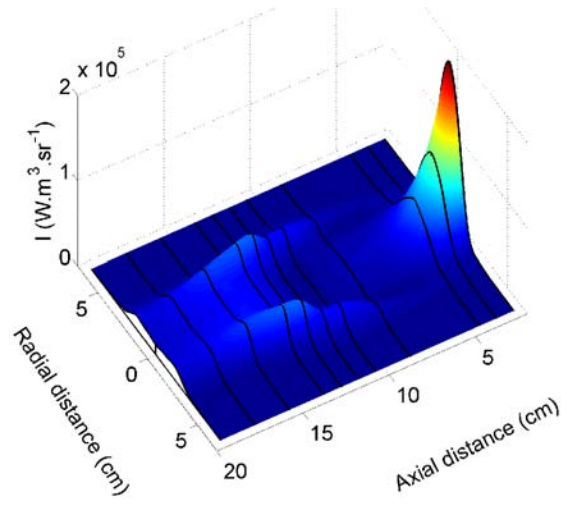
Figure 6. *Atomic contribution [400-900]nm - 6 mbar back pressure.*

Figure 7. *Atomic contribution [400-900]nm - 12 mbar back pressure.*

3. SPECTROSCOPIC DIAGNOSTICS

3.1. Excited electronic states distribution

Measured emission ϵ_{ul} of atomic transition allows a straight probing of the upper (emitting) level n_u population density through the relation:

$$\epsilon_{ul} = n_u \frac{A_{ul}}{4\pi} \frac{hc}{\lambda_{ul}} \quad (W.m^{-3}.sr^{-1}), \qquad (1)$$

where A_{ul} (s^{-1}) is the Einstein coefficient associated to spontaneous emission from level u to level l respectively of energy E_u and E_l. λ_{ul} designates the line position. Assuming Local Thermodynamic Equilibrium (LTE), the internal level population density of a level u of energy

E_u and degeneracy g_u follows the Boltzmann distribution ruled by a single temperature T_{LTE} given by:

$$n_u(T_{LTE}) = N(T_{LTE})\frac{g_u exp\left(-\frac{E_u}{k_B T_{LTE}}\right)}{Q_{int}(T_{LTE})} \quad (m^{-3}),$$

(2)

where species concentration N (m^{-3}) and internal partition function Q_{int} are calculated at equilibrium. The
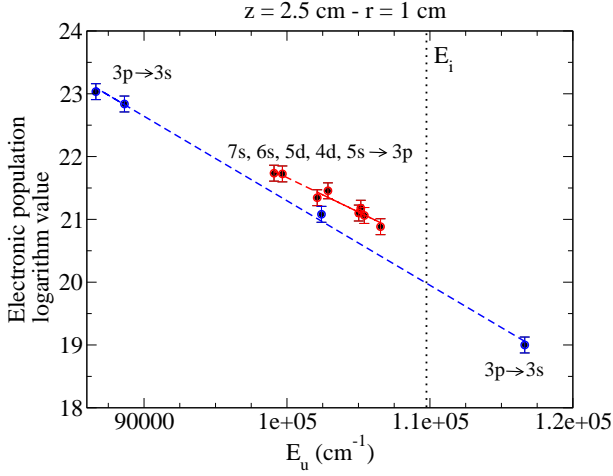

Figure 8. Boltzmann diagram at the center of the jet using oxygen atomic lines (r = 0 cm, z = 2.5 cm).

lack of information about the static pressure distribution within supersonic flows prevent from investigating absolute population. Relative population distribution of atomic excited states will be examined through the so-called Boltzmann diagram. In thermal plasmas, atomic state distribution function obeys Boltzmann equilibrium and the excitation temperature T_{exc} is evaluated on the basis of the Boltzmann diagram method. This approach is convenient as no assumption is made concerning the species concentration. The upper level density being straightly related to emission through relation (1), it is expressed in terms of T_{exc} combining equations (1) and (2) in the form:

$$ln\left(\frac{n_u}{g_u}\right) = -\left(\frac{1}{k_b T exc}\right)E_u + ln\left(\frac{N}{Q_{int}}\right). \quad (3)$$

Excitation temperature T_{exc} is directly obtained from the slope of a straight line fitted on the set of experimental electronic excited states population logarithm values (left term of Equation 3). On figure 8, typical Boltzmann diagram using oxygen atomic lines is displayed. As the spectral window cover by the upper emitting levels of nitrogen lines is narrow, the study will focus only on oxygen lines. No obvious deviation from Boltzmann distribution has been detected. Although a slight dispersion of measured population around the linear regression is observed, the excitation temperature will be derived from the set of thirteen oxygen lines displayed in the appendix.

3.2. Stark broadening of Hydrogen lines

The determination of the electron density is executed though the fitting of calculated hydrogen Stark broadened lines onto experimental data. Calculation of the the Stark broadened line profiles have been reported in literature for the first three Balmer lines of hydrogen (H_α, H_β and H_γ). Well known databases are elaborated using different theoretical models named as quasi-static ion approximation model (VCS)[C. 73], Model Microfield Method (MMM)[B. 01] and Computer Simulation (CS)[M. 03]. In this study, a favor is given to CS model as its up-to-date database allows to account for air mixture using reduced mass coefficient. The available parameters range belonging to this model are presented in table 1. In figure 9,

Model	Constraint on N_e (cm^{-3})	Constraint on T_e (K)
CS	$10^{14} \leq N_e \leq 10^{19}$	$1042 \leq T_e \leq 1.7 10^{6}$

Table 1. Plasma parameters validity range.

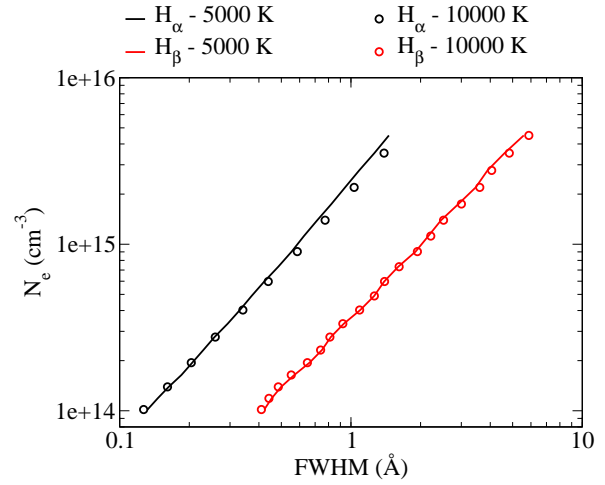*Figure 9. H_α and H_β FWHM from Gigosos & al. CS simulations [M. 03].*

electron density evaluated using CS model is plotted as a function of the Full Width at Half Maximum (FWHM) of H_α and H_β lines in the density range of interest. It shows that for the temperature range of interest, the influence of electron temperature on the FWHM is negligible. It has been also verify that the entire lineshape is not affected by the electron temperature. In CS database, line half-profiles are available in the form of tables where values of intensity are tabulated against wavelengths for certain values of electron temperature T_e and density N_e. In order to obtain a profile for any couple (T_e,N_e), a bilinear interpolation is performed from theoretical data. The theoretical line profile is convoluted with the instrumental broadening of the apparatus and Doppler broadening is assumed negligible. The program interpolates points from the theoretical line profile to match the grid of the experimental data set. Any background in the experimental data is zeroed so that the data is directly comparable

to the theoretical profiles. Typical fittings obtained using this procedure are displayed in 10.
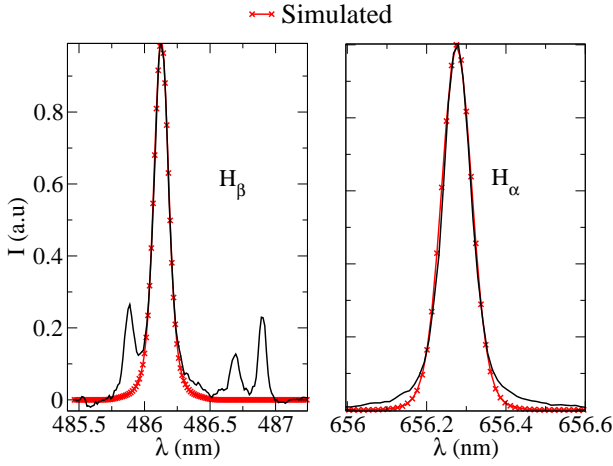

Figure 10. Hydrogen lineshape fitting.

3.3. Rotational temperature

Plasma characterization using molecular spectra is done on the basis of common fitting approaches consisting of the minimization of the functional defined by the Root Mean Square Error (RMSE) between the experimental spectrum and the spectrum calculated under various equilibrium assumptions. The theoretical spectra required to determine the RMSE are calculated on the basis of an advanced tool developed and available at the EM2C laboratory and so-called High Temperature Gas Radiation (HTGR) code [M. 08]. Assuming thermal equilibrium, the temperature $T_{thermal}$ is obtained applying the fitting procedure on experimental spectra normalized to unity, which consist in the minimization of the functional expressed as:

$$RMSE\left(T_{thermal}\right) = \sqrt{\frac{1}{N}\sum_{i=1}^{N}\left(\bar{S}_{\lambda_i}^{exp} - \bar{S}_{\lambda i}^{theo}(T_{thermal})\right)^2} \quad (4)$$

where $\bar{S}_{\lambda_i}^{exp}$ (resp. $\bar{S}_{\lambda_i}^{theo}$) designates the normalized experimental spectrum (resp. calculated spectrum) and N is the number of experimental points in the considered spectral range. The HTGR code can support various assumption concerning the distribution of emitting levels or the number of species accounted. In this study, the fitting will be performed accounting for three molecular system belonging to N_2^+, N_2 and CN species assuming thermal equilibrium and chemical nonequilibrium. In this situation, the minimization is expressed as:

$$RMSE\left(T_{thermal}, \alpha_1, \alpha_2\right) = \sqrt{\frac{1}{N}\sum_{i=1}^{N}\left(\bar{S}_{\lambda_i}^{exp} - \bar{S}_{\lambda i}^{theo}(T_{thermal,\alpha_1,\alpha_2})\right)^2} \quad (5)$$

where α_1 (resp. α_2) stands for the chemical non equilibrium factor $\alpha_1 = \frac{N_{N_2^+}}{N_{N_2}}\frac{Q_{int}(N_2)}{Q_{int(N_2^+)}}$ (resp. $\alpha_2 = \frac{N_{N_2^+}}{N_{CN}}\frac{Q_{int}(N_{CN})}{Q_{int}(N_2^+)}$). Typical best fit obtained using multi-
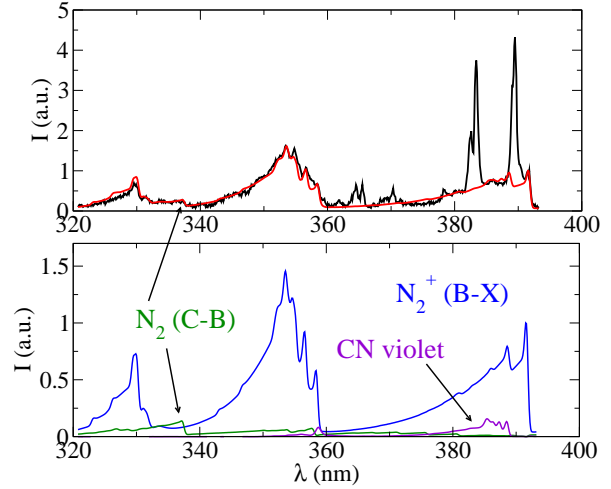

Figure 11. Multi-species best fit (top) and detailed species contribution (bottom).

species spectra calculation is displayed in figure 11. The fitting corresponds to measurement performed in the compression region (12 mbar case) at 9.5 cm from the nozzle exit. The robust method used for the fitting allows to fit three vibrational bands of N_2^+ First Negative system despite several atomic lines overlapping. The good agreement between measured and calculated spectra evidences for thermal equilibrium.

4. RESULTS

In figure 12 (resp. 13), excitation temperature and electron density radial profiles are plotted for 6 mbar (resp. 12 mbar) back pressure case at two axial positions in the expansion region. Black (resp.red) lines correspond to 2.5 cm (resp. 3.5 cm) axial position. Electron density profiles determined using both H_α and H_β lines show good agreement. For clarity, only profiles determined from H_β line are displayed. We assume that the main source of uncertainty on the electron density determination is due to the measured apparatus function. Therefore electron density profiles are displayed assuming $+/-5\%$ error on the apparatus function. Strong recombining situation is clearly evidenced at the jet centerline in figure 12. Indeed, having similar excitation temperature for both axial locations, a significant disagreement is observed in electron density value. As an indication, for 15 mbar air plasma at LTE, equivalent drop in electron density should be accompanied by 12 % drop in temperature [B. 96]. This recombining state is no more occurring on the edge where temperature and density match for both axial locations. Oppositely, in figure 13 recombining situation
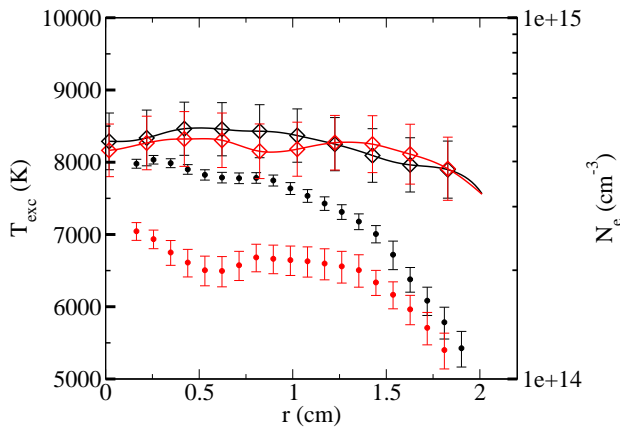
Figure 12. Radial profiles - z = 2.5 cm (black), z = 3.5 cm (red). Excitation temperature (diamonds), electron density (circles). 6 mbar back pressure.

Figure 14. Axial profiles - r = 1.0 cm. Excitation temperature (diamonds), electron density (circles). 6 mbar back

Figure 13. Radial profiles - z = 2.5 cm (black), z = 3.5 cm (red). Excitation temperature (diamonds), electron density (circles). 12 mbar backpressure.
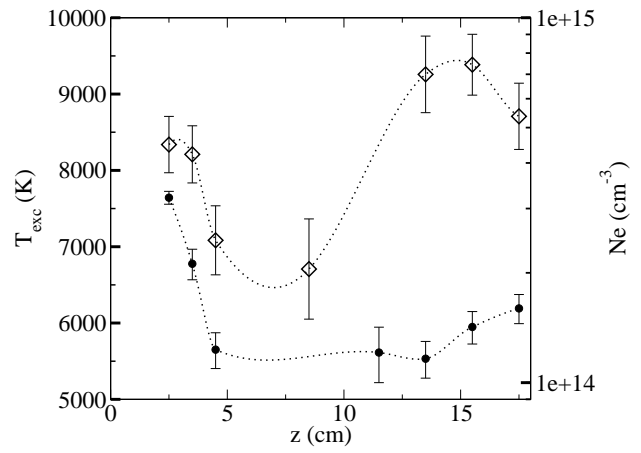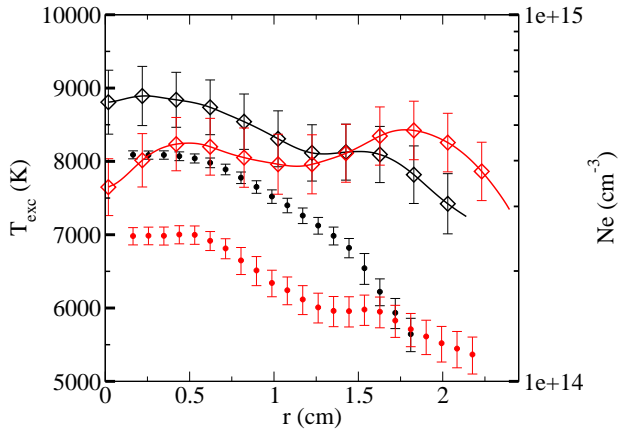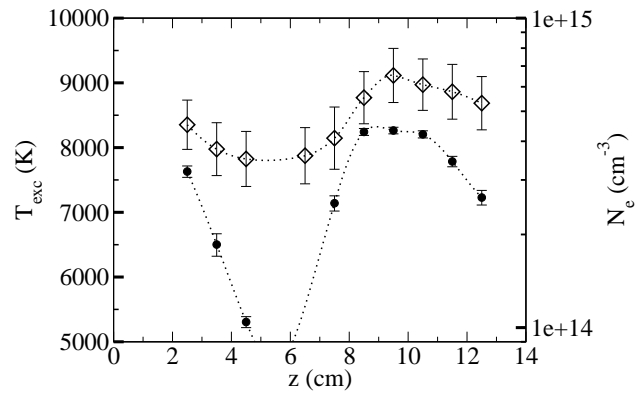

Figure 15. Axial profiles - r = 1.0 cm. Excitation temperature (diamonds), electron density (circles). 12 mbar back pressure.

is much less significant at the jet centerline. Following the same argument, at 3.5 cm axial location, the outer part of the jet corresponding to the barrel shock (from 1.5 cm radial distance) evidences an ionizing situation. Complex hydrodynamic structure lead to various thermodynamic non equilibrium situations and radial gradients have to be carefully accounted when analyzing axial profiles. In figure 14 (resp. 15), excitation temperature and electron density axial profiles are plotted for 6 mbar (resp. 12 mbar) back pressure. The radial position was chosen at 1.0 cm from the jet axis in order to get significant number of point on the profile. Indeed, electron density lower than 1.0^{14} cm$^{-3.}$ cannot be determined using CS model and low atomic contribution at several locations prevent from a full radial profile determination. Both figures cannot be directly compared as radial gradients play an important role. Electron density and excitation temperature profiles shows coherent variations in the expansion zone. Huge error bar at the end of the expansion region in the

6 mbar back pressure case denotes an important dispersion of atomic excited states around linear regression and the use multiple excitation temperatures might be relevant for further analysis. After the Mach disk, electron density is increasing faster in 12 mbar back pressure case. In 6 mbar back pressure case, electron density and excitation temperature profiles in the compression region are decorrelated. Further analysis is possible by investigating the rotational temperature. Rotational temperature in the compression region for 12 mbar back pressure case is presented in figure 16 with the associated chemical non equilibrium factor for CN species (concentration of N_2 species being found negligible). Temperature profile is coherent with hydrodynamics structure of the jet. The slope of the chemical nonequilibrium factor of CN should be opposite to the slope of temperature which is the case on the edge of the jet because of plasma cooling. However in the shear layer, the concentration of CN species increases as the temperature increases which denotes for a nonequilibrium situation.
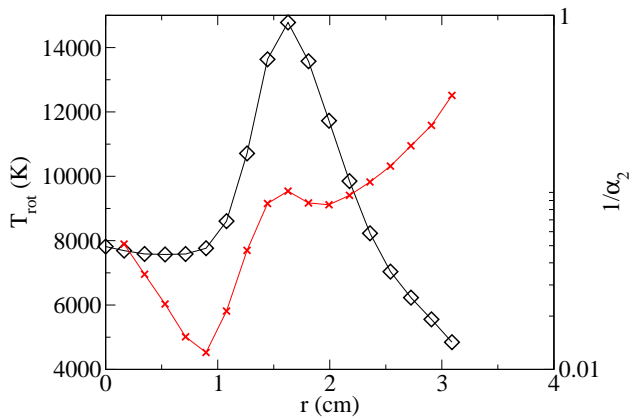
Figure 16. Radial profiles - z = 9.5 cm. Rotational temperature (black) and chemical non equilibrium factor for CN (red).

5. CONCLUSION

A qualitative description of supersonic jet structure was performed through Abel inverted raw images corresponding to underexpanded and highly unerexpanded cases. Various spectroscopic diagnostics have been used to characterize these plasma flows in the first expansion-compression zone. Preliminary results are encouraging and point out the main characteristics of supersonic plasma jets. Electron number density was determined by fitting experimental hydrogen lines onto theoretical lineshape. Atomic excited states distribution have been measured for oxygen atomic lines and evidences that Boltzmann assumption was valid in most regions of the jet. However, at the end of the expansion region, an important dispersion of atomic excited states around linear regression was evidenced and the use multiple excitation temperatures might be relevant for further analysis. At the jet centerline, the expansion of the plasma is accompanied by a rapid cooling and recombination which results in kinetic non equilibrium between electrons and heavy particles. Oppositely, shear layers are location of ionizing situation with presence of molecular radiation. The determination of rotational temperature has been performed where molecular spectra of N_2^+ First Negative system are suitable for fitting procedure. Preliminary analysis on rotational temperature are in agreement with hydrodynamic structure of the jet and permits to determine the evolution of CN species concentration. Further comparison with excitation temperature will allow to identify nonequilibrium situations.

REFERENCES

[B. 96] B. J. McBride, S. Gordon. Computer program for calculation of complex chemical equilibrium compositions and application. II User manual and program description. *NASA Lewis Research Center, Cleveland, OH*, Reference publication 1311, 1996.

[B. 97] B. Bottin, M. Carbonaro , S. Zemsch and G. Degrez. Aerothermodynamic design of an inductively coupled plasma wind tunnel. *32nd AIAA Thermophysics Conference, Atlanta, USA*, AIAA paper 97-2498, June 23-25 1997.

[B. 00] B. Bottin, O. Chazot, M. Carbonaro, V. Van Der Haagen and S. Paris. Measurement techniques for high enthalpy and plasma flows. *RTO-EN-8*, AC/323(AVT)TP/23,8, 2000.

[B. 01] B. W. Acon, C. Stehle, H. Zhang, A. Montaser. Stark-broadened hydrogen line profiles predicted by the model microfield method for calculating electron number densities. *Spectrochimica Acta Part B*, Vol. 56:pp. 527–539, 2001.

[C. 73] C. R. Vidal, J. Cooper, E. W. Smith. Hydrogen Stark-Broadening Tables. *The Astrophysical Journal supplement*, Vol. 214, 1973.

[D. 08] D. J. Drake, S. Popovic, L. Vuskovic. Characterization of a supersonic microwave discharge in Ar/H2/Air mixtures. *J. Appl. Phys.*, 104, 2008.

[D. 09] D. J. Drake, S. Popovic, L. Vuskovic. Characterization of a CO2/N2/Ar supersonic flowing discharge. *J. Appl. Phys.*, 106, 2009.

[L.R94] L.Robin, P.Vervisch, B.G.Cheron. Experimental study of a supersonic low-pressure nitrogen plasma jet. *Phys. Plasma*, Vol.1 - NO.2:pp.444–458, 1994.

[M. 03] M. A. Gigosos, M. A. Gonzalez, V. Cardenoso. Computer simulated Balmer-alpha, -beta and -gamma Stark line profiles for non-equilibrium plasmas diagnostics. *Spectrochimica Acta Part B*, Vol. 58:pp. 14891504, 2003.

[M. 08] M. Y. Perrin, P. Rivière, A. Soufiani. Radiation database for Earth and Mars entry. *Von Karman Lecture Series*, RTO-EN-AVT-162, 2008.

[M.C93] M.C.M.van de Sanden, J.M.de Regt, D.C.Schram. Recombination of argon in an expanding plasma jet. *Physical review E*, Vol.47-Number 4, April 1993.

[NIS] NIST atomic spectra database . *http://physics.nist.gov/PhysRefData/ASD/index.html*.

[S.E01] S.E.Selezneva, M.Rajabian, D.Gravelle, M.I.Boulos. Study of the structure and deviation from equilibrium in direct current supersonic plasma jets. *J. Phys. D: Appl. Phys.*, Vol.34:pp.2862–2874, 2001.

[V.S02] V.Sember, D.V.Gravelle, M.I.Boulos. Spectroscopic study of a supersonic plasma jet generated by an ICP torch with a convergent-divergent nozzle. *Journal of Physics D: Applied Physics*, Vol.35:pp.1350–1361, 2002.

APPENDIX

O lines			$D_e = 109837.02 cm^{-1}$		
394.7295	$4.91 10^5$	73768.200	99094.837	5	7
394.7481	$4.88 10^5$	73768.200	99093.641	5	5
394.7586	$4.87 10^5$	73768.200	99092.968	5	3
436.8258	$7.58 10^5$	76794.978	99680.968	3	3
436.8193	$7.56 10^5$	76794.978	99681.309	3	1
436.8242	$7.59 10^5$	76794.978	99681.049	3	5
501.8782	$4.28 10^5$	86 625.757	106 545.354	3	5
501.9291	$7.13 10^5$	86 627.778	106 545.354	5	5
543.5178	$7.74 10^5$	86625.757	105019.307	3	5
543.5775	$1.29 10^6$	86627.778	105019.307	5	5
543.6862	$1.80 10^6$	86631.454	105019.307	7	5
595.8386	$6.80 10^5$	88630.587	105409.008	3	5
595.8386	$3.78 10^5$	88630.587	105409.008	3	3
595.8584	$2.27 10^5$	88631.146	105409.008	5	5
595.8584	$2.52 10^4$	88631.146	105409.008	5	3
595.8584	$9.06 10^5$	88631.146	105409.008	5	7
604.6233	$1.05 10^6$	88630.587	105165.232	3	3
604.6438	$1.75 10^6$	88631.146	105165.232	5	3
604.6495	$3.50 10^6$	88631.303	105165.232	1	3
615.5971	$5.72 10^6$	86625.757	102865.655	3	3
615.6778	$5.08 10^6$	86627.778	102865.547	5	7
615.8187	$7.62 10^6$	86631.454	102865.506	7	9
645.360	$1.65 10^6$	86625.757	102116.698	3	5
645.444	$2.75 10^6$	86627.778	102116.698	5	5
645.598	$3.85 10^6$	86631.454	102116.698	7	5
700.1899	$1.47 10^6$	88630.587	102908.489	3	3
700.1922	$2.65 10^6$	88630.587	102908.443	3	5
700.2173	$9.83 10^4$	88631.146	102908.489	5	3
700.2196	$8.83 10^5$	88631.146	102908.443	5	5
700.2230	$3.53 10^6$	88631.146	102908.374	5	7
700.2250	$1.96 10^6$	88631.303	102908.489	1	3
715.670	$5.05 10^7$	102662.026	116631.094	5	5
725.4154	$2.24 10^6$	88630.587	102411.995	3	3
725.4448	$3.73 10^6$	88631.146	102411.995	5	3
725.4531	$7.45 10^5$	88631.303	102411.995	1	3
777.1944	$3.69 10^7$	73768.200	86631.454	5	7
777.4166	$3.69 10^7$	73768.200	86627.778	5	5
777.5388	$3.69 10^7$	73768.200	86625.757	5	3
844.6247	$3.22 10^7$	76794.978	88631.303	3	1
844.6359	$3.22 10^7$	76794.978	88631.146	3	5
844.6758	$3.22 10^7$	76794.978	88630.587	3	3

Table 2. Spectroscopic data of the considered O emission lines used for air plasma [NIS].